Liquefaction and flow behavior of a thermally decomposing removable epoxy foam

K. L. Erickson, S. M. Trujillo, K. R. Thompson, A. C. Sun,
M. L. Hobbs & K. J. Dowding
Engineering Sciences Center, Sandia National Laboratories, USA.

Abstract

Polymer foams are used to encapsulate units requiring thermal and mechanical isolation in engineered systems. At high temperature, these foams chemically decompose. Decomposing foams generally undergo charring or liquefaction processes, while evolving low molecular weight species into the vapor phase. Evolved gases and vapors can cause substantial pressurization of closed containers. During thermal decomposition, the physical and chemical behaviors of the foams are coupled and can significantly affect heat transfer rates to the encapsulated units. The behavior of foams that undergo liquefaction can vary greatly depending on both physical and thermal boundary conditions as well as on decomposition chemistry.

A removable, epoxy foam was recently developed. This foam undergoes liquefaction during thermal decomposition. Decomposition chemistry and liquefaction processes are being investigated experimentally to provide a basis for developing predictive models. Multiple techniques and diagnostics are used to characterize physical and chemical behavior over a broad range of sample sizes and physical and thermal boundary conditions. For example, at the laboratory scale, 1-mg to 10-mg samples are used in TGA-FTIR and DSC experiments to determine decomposition chemistry and associated enthalpy changes. At the "production scale," 50 g to 100 g samples are used in high-temperature (~900° C) thermal response experiments, in which foam regression and liquefaction are examined using x-ray imaging. Foam regression away from a heated surface generally involves two moving boundaries, a fluid-solid interface and a fluid-vapor interface. In the simplest cases involving well-vented samples, both interfaces are relatively planar and regress in a one-dimensional fashion. Similar experiments involving totally confined samples produce complicated three-dimensional interfaces as a result of erosive channeling by hot vapors and fluids.

1 Introduction

Polymer foams are used to encapsulate units requiring thermal and mechanical isolation in engineered systems. At high temperature, these foams chemically decompose. Decomposing foams generally undergo charring or liquefaction processes, while evolving low-molecular-weight species into the vapor phase. Evolved gases and vapors can cause substantial pressurization of closed containers. During thermal decomposition, the physical and chemical behaviors of the foams are coupled and can significantly affect heat transfer rates to the encapsulated units. The behavior of foams that undergo liquefaction can vary greatly depending on both physical and thermal boundary conditions as well as on decomposition chemistry.

A removable, epoxy foam (REF) was recently developed [1]. This foam undergoes liquefaction during thermal decomposition. Decomposition chemistry and liquefaction processes are being investigated experimentally to provide a basis for developing predictive models. A variety of techniques and diagnostics are used to characterize the physical and chemical behavior of the foam over a broad range of sample sizes, as well as physical and thermal boundary conditions. For example, at the "laboratory scale," 1-mg to 10-mg samples are used in TGA-FTIR and DSC experiments to determine decomposition chemistry and associated enthalpy changes. At the "production scale," 50 g to 100 g samples are used in high-temperature (~900° C) thermal response experiments, in which foam regression and liquefaction are examined using x-ray imaging. Similar work with rigid polyurethane foam was reported previously [2].

This paper briefly summarizes results from both laboratory- and production-scale experiments. Emphasis is on results from the production-scale experiments and on the relationship between those results and foam decomposition chemistry, as well as the influence of physical and thermal boundary conditions.

2 Experiment

The two types of experiments are described below: production-scale and laboratory-scale.

2.1 Production-scale experiments

The configurations for all of the production-scale experiments to be discussed were similar. The basic features of all of the experiments are shown schematically in Fig. 1. Variations among experiments are described below and primarily involved the length of the foam sample, sample orientations, which are illustrated in Fig. 2, venting and pressurization, the maximum temperature of the heated plate, and the bulk density of the foam.

Transactions on Engineering Sciences vol 43, © 2003 WIT Press, www.witpress.com, ISSN 1743-3533

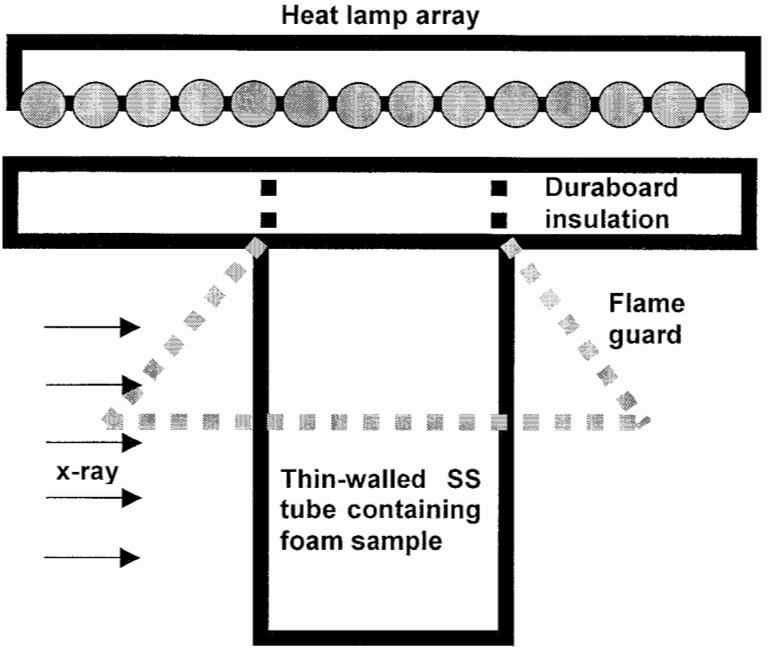

Figure 1: Schematic diagram of configuration for production-scale experiments.

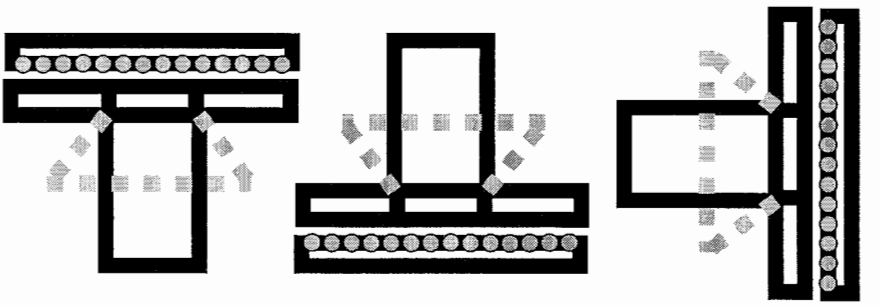

Figure 2: Sample orientations: (a) upright, (b) inverted, and (c) side.

Four sample container designs were used in the experiments. The common basis for each design (see Fig. 1) is the insertion of a foam cylinder into a sleeve, which was then sealed at each end with either a welded plate or a low-temperature-cure epoxy (in early tests, some containers were not sealed at the unheated end). Variations in the design include the number and size of vent/pressure-transducer ports near the top (heated) surface of the container; sample and container length; and the inclusion of internal masses simulating encapsulated objects. In each design, the sleeve was 88.9-mm (3.5-inch) OD, 0.508-mm (0.020-inch) wall thickness 321 SS tubing. Metal end plates were fabricated from 304 SS stock. The top surface of each container was painted on both sides (interior and exterior) with Pyromark™ 2500 series black paint to ensure consistent and uniform radiative properties. The foam insert was manufactured oversized and then machined for a snug fit in the sleeve. If internal temperature measurements in the foam were sought, the foam blank was machined to fit in the sleeve, and then instrumented prior to insertion. Sample dimensions and construction details are summarized in Table 1.

Seventeen quartz lamps were used to heat the samples. Each lamp is 9.53 mm (0.375 inch) diameter and 300 mm (11.8 inches) long with a maximum power rating of 6 kW. The 17 lamps were spaced 16 mm (0.625 inch) apart to form an array that was approximately 30 cm square. The lamps were mounted in a water-cooled aluminum holder with a polished surface behind the lamps. A maximum of 480 volts were supplied to the lamps through phase-angle fired Silicon Controlled Rectifiers with a maximum capacity of 1000 Amperes. Rigid insulation 25.4 mm (1 inch) thick with a 89-mm diameter hole located in the middle of the board was placed 38 mm (1.5 inch) from the lamps. The foam container was positioned 5.7 cm (2.25 inches) from the lamps at the back of the insulation board and aligned with the hole.

Temperature measurements were made with ungrounded, 0.81-mm (0.032-inch) diameter Inconel-sheathed K-type thermocouples. Pressure data were acquired using Setra model 206 or Ashcroft model K1 transducers. Temperature and pressure data were acquired at nominally 0.1 Hz using a LabView™-based data acquisition system.

The foam inside the sample container was imaged using a single- or two-x-ray camera system. The x-ray units were Philips 225 systems operated at 140kV and 15mA. In the two-camera case, the separation angle between the camera views was nominally 60°. The X-ray image frame rate was 0.2 Hz.

Table 1: Production-scale experiment details

	"AF"	"Series 2"	"Tuna"	"X-FER"
Foam Sample Length	108 mm (4.5 in.)	108 mm (4.5 in.)	50.4 mm (2 in.)	63.5 mm (2.5 in.)
Thickness of top (heated) surface (304 SS)	9.53 mm (0.375 in.)	9.53 mm (0.375 in.)	4.76 mm (0.188 in.)	9.53 mm (0.375 in.)
Number and ID of vent/pressure-transducer tubes	4 @ 6.35-mm holes (no tube)	4 @ 3.2 mm (0.125 in.)	1 @ 1.6 mm (0.063 in.)	2 @ 3.2 mm (0.125 in.)
Lower seal material and thickness	Unsealed, or epoxy sealed, ~6 mm (0.25 in.)	Epoxy, ~6 mm (0.25 in.)	304 SS, 3.2 mm (0.125 in.)	304 SS, 9.53 mm (0.375 in.)
Comments / Design details	Flame guard fitted over forward end of container; 2001	2002	Samples designed to investigate effects of pressurization; 2002	Semi-solid internal mass attached to lower seal plate; 2003

2.2 Laboratory-scale experiments

Laboratory-scale experiments have consisted primarily of thermal gravimetric analysis (TGA), often with concurrent evolved-gas analysis by Fourier transform infrared spectroscopy (FTIR), high-pressure thermal gravimetric analysis (HPTGA), differential scanning calorimetry (DSC), and use of a high pressure cell to examine pressures generated during decomposition of foam samples at moderate temperatures up to 300° C. A complete discussion of the various techniques and associated results are beyond the scope of this paper. However, the TGA-FTIR experiments are important to discussion of the results from the production-scale experiments and, therefore, are briefly described below.

The experimental arrangement for the TGA experiments is shown schematically in Fig. 3. The thermal gravimetric analyzer (TA Instruments Model 2950) consists of a microbalance, from which a sample pan, containing a foam sample, is suspended into a temperature-programmed furnace. The microbalance measures the sample mass as a function of time during decomposition. A thermocouple in close proximity to the sample pan indicates the sample temperature. A purge gas, usually nitrogen, sweeps decomposition gases and vapors from the surface of the sample.

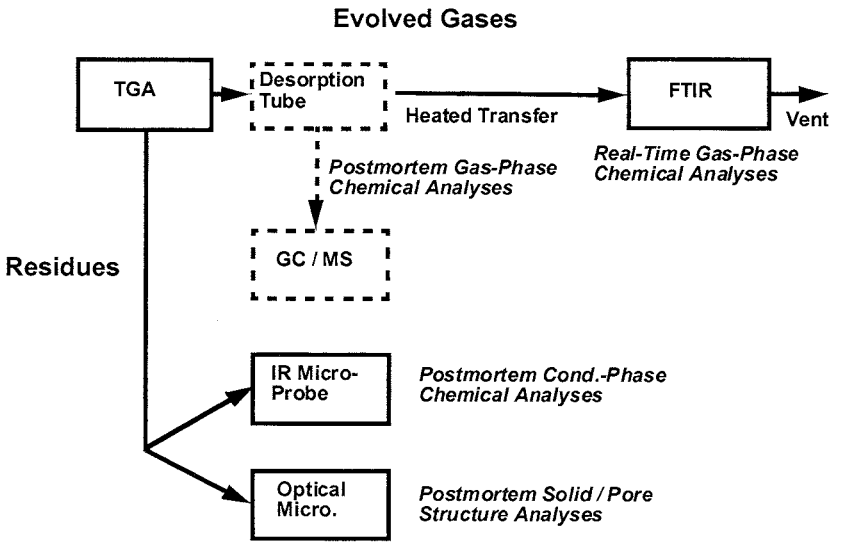

Figure 3: Schematic diagram of TGA-FTIR experiments.

TGA experiments with small (about 4- to 8-mg) samples were done in unconfined and partially confined sample configurations. The unconfined configuration involved samples in open platinum pans and was used to examine initial decomposition mechanisms under conditions that minimize effects of mass transfer and reversible and secondary reactions. The partially confined configuration involved sealed hermetic aluminum pans (TA Instruments) having lids with circular orifices as small as 0.06 mm and was used to examine the effects of any reversible or secondary reactions that would result from limiting mass transfer of the decomposition products away from the sample.

Analysis of the gases that evolved from the samples, in either unconfined or partially confined configuration, most frequently was done with real-time FTIR spectroscopy, as shown schematically in Fig. 3. The purge gas (typically 50 to 60 cc/min UHP N_2) from the TGA furnace flowed through a heated stainless steel transfer line (maintained at 250 to 300° C) to the TGA-FTIR Interface Unit in an Auxiliary Experiment Module (maintained at 300° C) of a Nicolet Magna 750 FTIR Spectrometer.

An alternative technique, illustrated schematically by the dashed portion of Fig. 3, was used in selected experiments to obtain additional information for identifying several of the evolved gas species. In the alternative technique, periodic sampling of evolved gases was done using thermal desorption tubes connected directly to the exhaust from the TGA Furnace. The effluent end of the desorption tube was either vented or connected to the heated transfer line to the TGA-FTIR Interface Unit. Gas samples were collected on desorption tubes packed with Tenax TA, 60/80 mesh. In this case, the purge gas flow rate was approximately 30 cc/min. The desorption tubes were capped and placed in a Perkin-Elmer

ATD400 Automated Thermal Desorption unit that was directly connected to a Finnigan GCQ gas chromatograph/ion trap mass spectrometer. The ATD400 is equipped with a Perkin-Elmer low-flow VOC trap for organic vapor concentration. The desorption tubes were heated to 350° C to collect the sample gases on the trap. The trap was then heated to 350° C to introduce the sample to the GCQ. The split ratio from the ATD400 was 40.6/1.3. The gas chromatography column used was a J&W DB-5ms 30 m x 0.25 mm capillary column, 1.0 μm film thickness. The GC heating profile was 40° C for 7 minutes, then a 20 °C/min ramp to 295° C, with a 5 minute hold at 295° C. The mass spectrometer was used in the electron ionization mode (70 ev); one full scan per second was collected from mass 33 to 380. The filament delay time was 4.33 minutes.

3 Results

3.1 Production-scale experiments

Specific details of the configurations used in the four types of production-scale experiments discussed below were summarized in Table 1.

3.1.1 Material relocation resulting from liquefaction and flow due to gravity

X-ray images from two "AF" series experiments (see Table 1) in upright and inverted orientations (see Fig. 2) are shown in Figs. 4 and 5, respectively. Images from a "Series 2" experiment in the side orientation are shown in Fig. 6. The sample containers in Figs. 4-6 were vented directly under the heated plate, so that significant pressure gradients would not develop along the axis of the cylindrical foam sample. However, liquefaction occurred during foam decomposition, presumably because the products forming the liquid were accumulating faster than they could vaporize. Also, the accumulating decomposition products may have dissolved some of the partially decomposed foam. As the fluid phase forms, flow occurs under the influence of gravity.

The power to the heat lamps was controlled so that the temperature of the heated plate was ramped (about 200° C/min) to a set point of 750° C and was maintained at that temperature for the duration of the experiment. The bulk density of the foam samples was nominally 0.12 g/cm^3 (8 lb/ft^3). The arrays of thin dark lines in the figures are the thermocouples that were imbedded in the foam and that were welded to the outside of the container.

Figure 4a shows the initial foam sample before heating in the upright orientation. The darker region in the upper portion of the figure resulted from the flame guard used to prevent ignition of the vented gases (see Fig. 1). In Fig. 4b, about 60 percent of the foam sample has regressed from the heated surface. A dark band of "bubbling" fluid has formed above the un-reacted foam. In Fig. 4c, the foam sample has almost completely regressed and a larger region of bubbling fluid has accumulated.

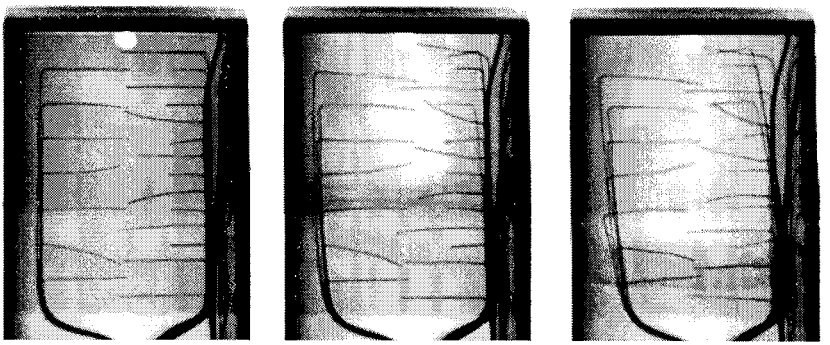

(a) (b) (c)

Figure 4: x-ray images from foam sample heated in upright orientation.

A similar series of x-ray images are shown in Fig. 5 for the inverted orientation. Figure 5a shows the initial sample. In Fig. 5b, the foam has only regressed a short distance into the sample, but a dome-shaped regression front has already developed. A thin dark region appears along the surface. A dark diffuse region appears to descend from the domed surface. This is probably a fluid phase moving under the influence of gravity. In Fig. 5c, the dome-like regression front is near the end of the foam sample, and a dark diffuse region is present along the sides of the container. However, no bubbling fluid layer has developed as in the upright orientation, Fig. 4.

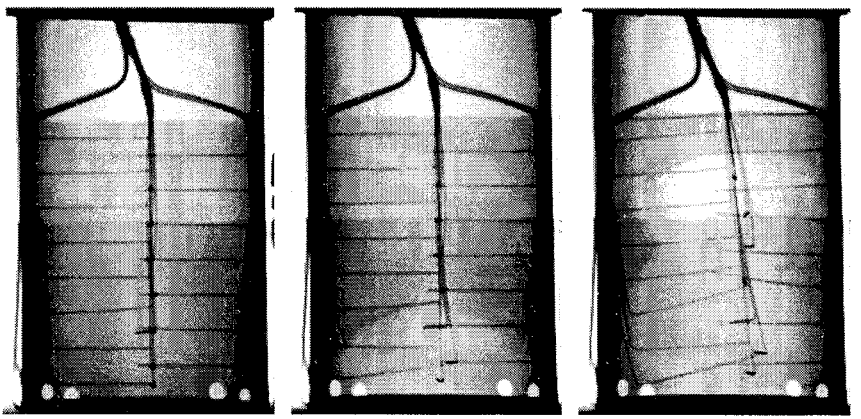

(a) (b) (c)

Figure 5: x-ray images from foam sample heated in inverted orientation.

Figure 6 shows a series of x-ray images from a foam sample heated in the side orientation. The heat flux from the lamps is incident from the right. In this case, the flame guard was removed and each vent hole was connected by stainless steel tubing to a manifold that removed decomposition products from the vicinity of the heat lamps. The vent on the underside of the can was capped. The other three vents were available to relieve gas pressure. Figure 6a shows the initial sample.

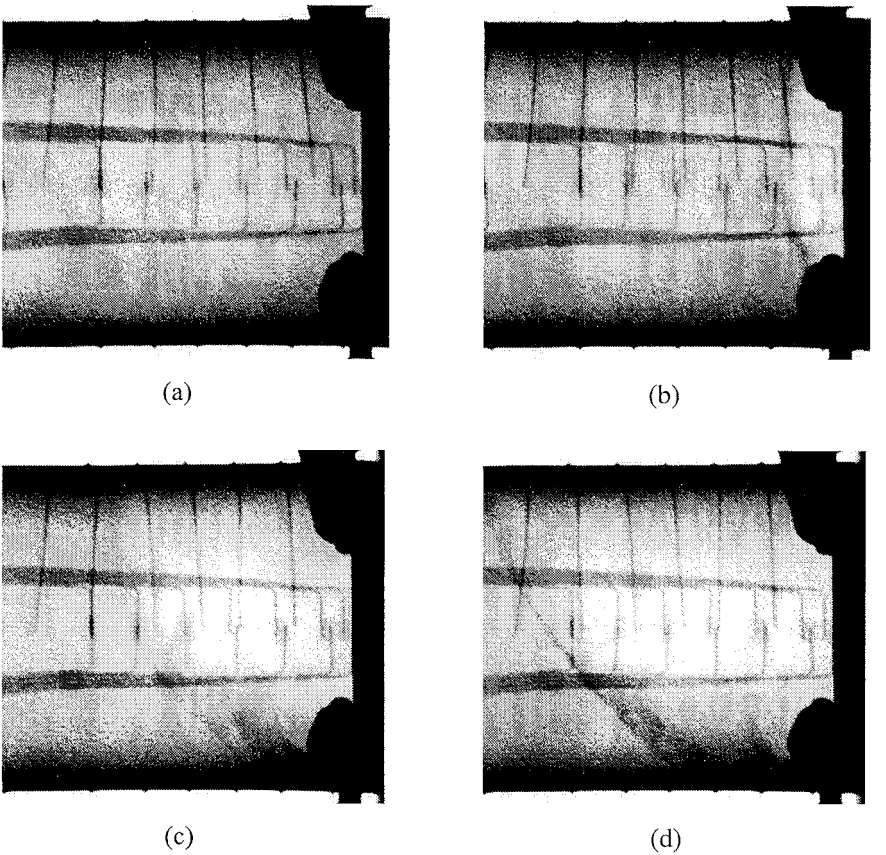

Figure 6: x-ray images from foam sample heated in the side orientation.

Figure 6b shows that the regression front is already asymmetric shortly after the onset of decomposition. As the foam continues to decompose, the regression front becomes increasingly asymmetric. In Figs. 6c and 6d, a dark diffuse region has formed along the slope of the regression front. This appears to be a fluid that is flowing down the regression front under the influence of gravity and collecting in the lower region of the container while the more volatile decomposition products evaporate.

3.1.2 Material relocation due to flow induced by a pressure gradient

Figures 7 and 8 show x-ray images from two experiments in the "Tuna" series (see Table 1). The images in Figs. 7 and 8 are shown for similar elapsed times.

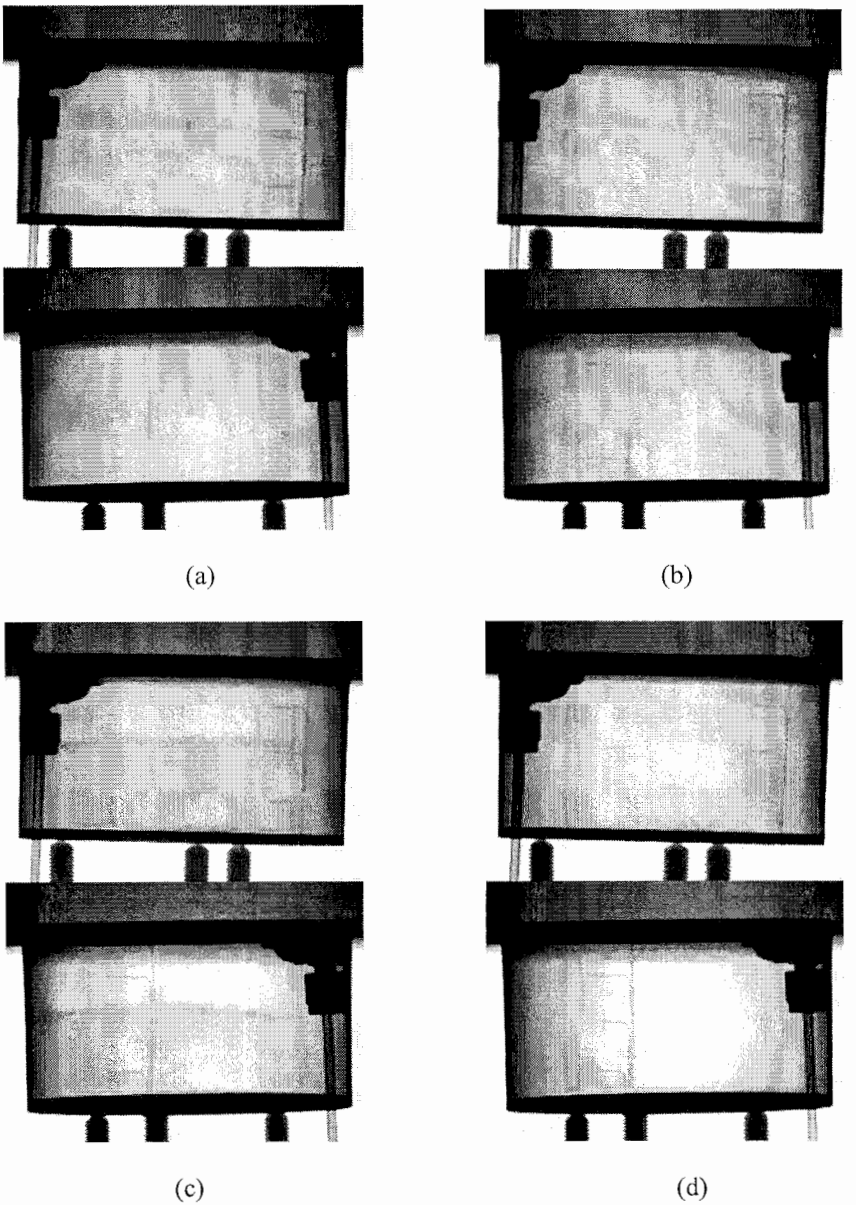

Figure 7: x-ray images from bottom-vented REF sample. Bulk density about 0.12 g/cm^3 (8lb/ft^3).

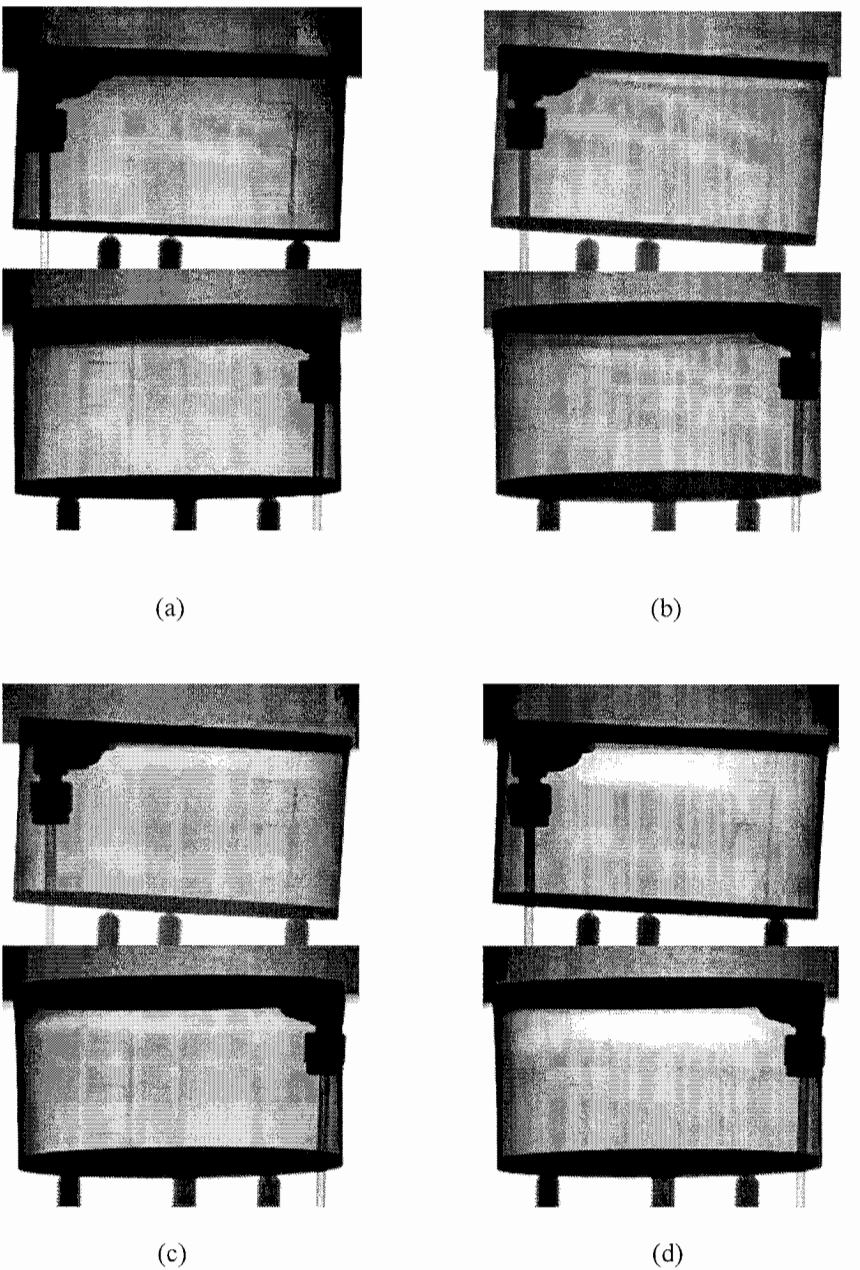

Figure 8: x-ray images from bottom-vented REF sample. Bulk density about 0.3 g/cm^3 (20 lb/ft^3).

In the "Tuna" series, two x-ray cameras were used. The cameras were separated by an angle of about 60 degrees. The images from the two cameras have been stacked in Figs. 7 and 8. The images in Fig. 7 are from a foam sample having a bulk density of about 0.12 g/cm^3 (8 lb/ft^3). The images in Fig. 8 are from a sample having a bulk density of about 0.3 g/cm^3 (20 lb/ft^3). Both experiments were done with the samples in the upright orientation as indicated in Fig. 9a. The only vent in the containers was a 1.6-mm (0.063-inch) hole in the bottom plate (Fig. 9a). Thermocouple locations are also shown in Fig. 9a. The pressure transducer responses for the samples in Figs. 7 and 8 are shown in Fig. 9b. The thermocouple responses from the samples in Figs. 7 and 8 are shown in Figs. 9c and 9d, respectively. The power to the heat lamps was controlled so that the temperature of the top plate was ramped (about 200° C/min) to a set point of 920° C and was maintained at that temperature for the duration of the experiment.

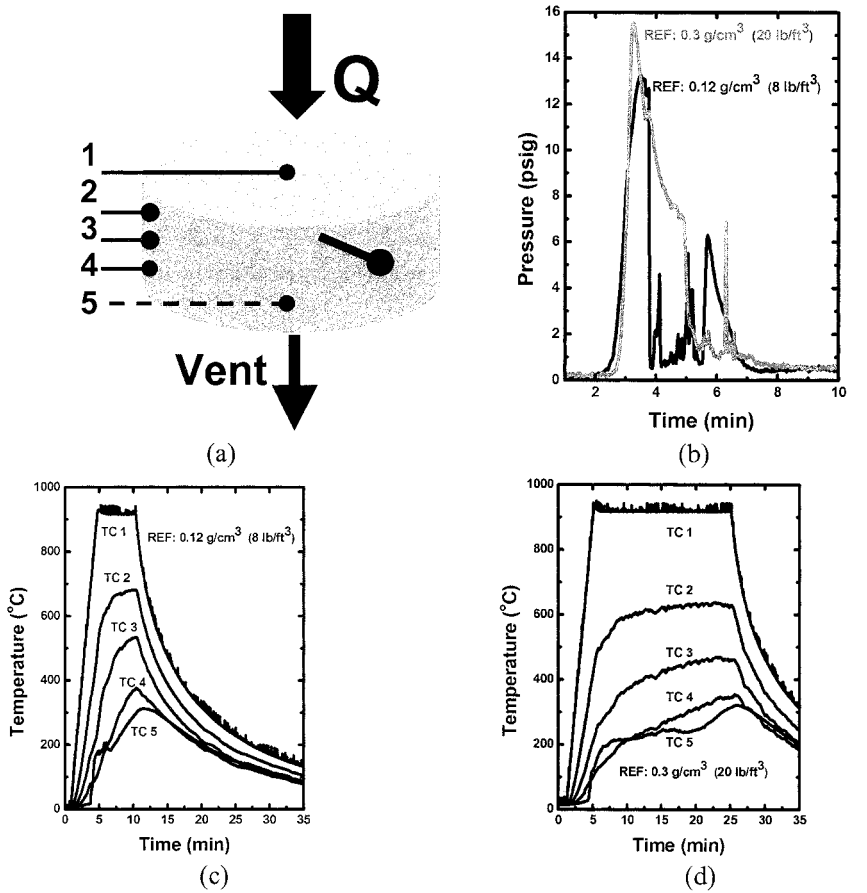

Figure 9: (a) Sample configuration for bottom-vented samples, (b) pressure transducer response, (c) thermocouple response for sample shown in Fig. 7, and (d) thermocouple response for sample shown in Fig. 8.

Figure 7a shows the initial sample. The thin dark region at the top of the container in Fig. 7b indicates the onset of decomposition. Figure 7c shows that the foam has regressed substantially. The foam has an eddy-like appearance, which is attributed to erosive channeling that is more visible in Fig. 8. Figure 7d shows that most of the foam has decomposed and vented through the bottom hole. Both a liquid and a vapor jet were observed issuing from the vent hole.

Figure 8a shows the initial sample of more dense foam. The darker region on the right of Figure 8b shows the erosive channel that forms during the initial decomposition and produces the eddy-like structures seen in Figs. 8c and 8d. The appearance of the erosive channel in Fig 8b corresponds in time to the drop in pressure that occurs between 3 and 4 minutes as shown in Fig 9b. An abrupt rise in TC 5, shown in Figs. 9c and 9d, also occurs as hot vapor begins exhausting through the vent between 4 and 5 minutes.

3.1.3 Material relocation (pressure gradient) and pressurization to failure

Figures 10 and 11 show x-ray images from two experiments in the "Tuna" series that were "totally confined" until the containers failed due to pressurization from the decomposition products. Again, two x-ray cameras were used and were separated by an angle of about 60 degrees. The images from the two cameras have been stacked in Figs. 10 and 11. The images in Fig. 10 are from a foam sample having a bulk density of about 0.12 g/cm^3 (8 lb/ft^3). The images in Fig. 11 are from a sample having a bulk density of about 0.3 g/cm^3 (20 lb/ft^3). Both experiments were done with the samples in the upright orientation as indicated in Fig. 9a. Thermocouple locations were also as shown in Fig. 9a. The pressure transducer responses for the samples in Figs. 10 and 11 are shown in Figs. 12a and 12b, respectively. The thermocouple responses from the samples in Figs. 10 and 11 are shown in Figs 12c and 12d, respectively. The power to the heat lamps was also controlled so that the temperature of the top plate was ramped (about 200° C/min) to a set point of 920° C and was maintained at that temperature for the duration of the experiments.

Figures 10a and 11a show the initial samples. Figures 10b and 11b show the onset of erosive channeling that appears to cause highly asymmetric and three-dimensional regression of the foam as decomposition occurs, as indicated in Figs. 10c, 10d, 11c, and 11d. Substantial pressurization of the containers occurred, as shown in Fig. 12a, and lead to failure. In the case of the lower-density sample (Fig. 10), the container failed violently. In the case of the higher-density sample (Fig. 11), the weld around the pressure tap failed, and the container gradually vented. The apparent channeling in the x-ray images corresponds temporally to the "plateau" in the pressure data between 3 and 4 minutes, shown in Fig. 12b. A corresponding jump in the temperatures from TC's 3 and 4, in Figs 12c and 12d, also occurs between about 4 and 5 minutes and further indicates channeling.

Figures 10 and 11 also show the effect of foam density on the regression rate. Erosive channeling occurs regardless of density. However, the more dense foam requires more time to completely decompose due to the additional mass, which requires more energy for decomposition.

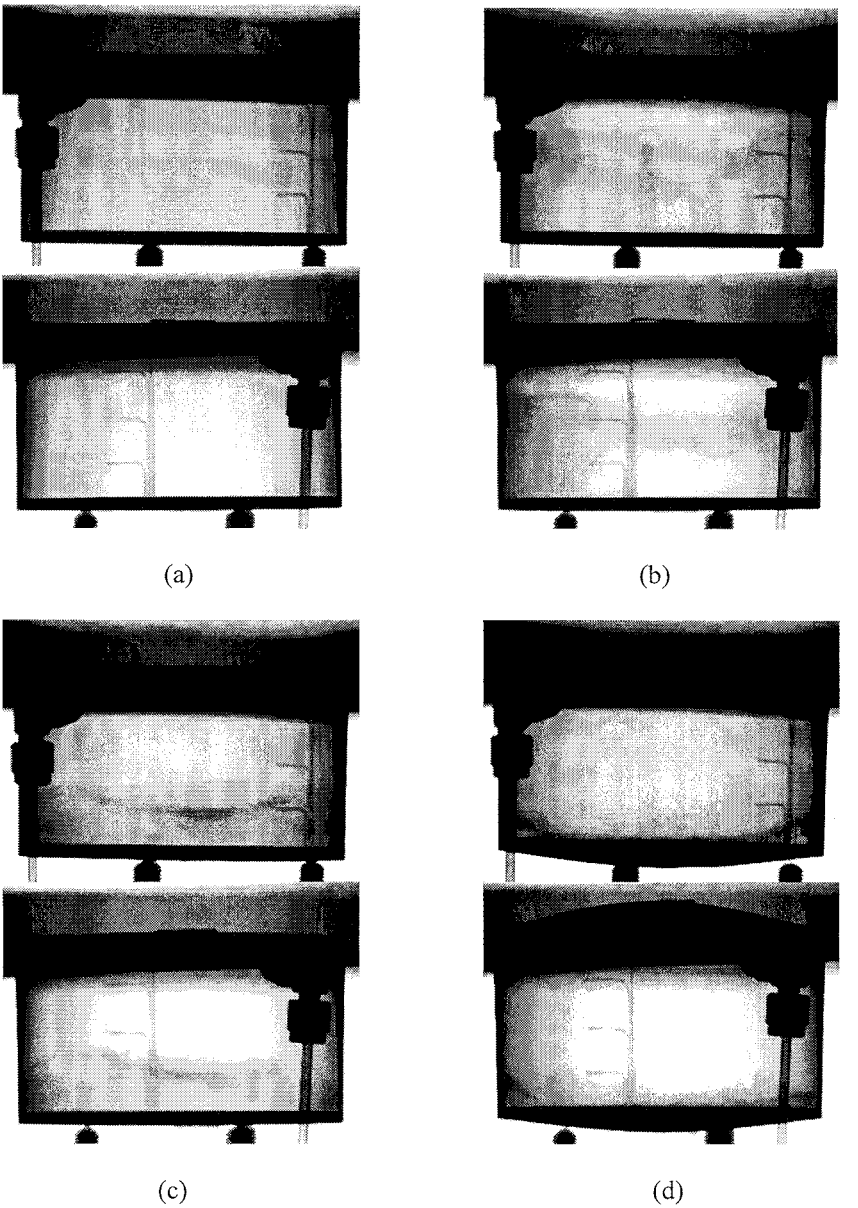

Figure 10: x-ray images from confined REF sample. Bulk density about 0.12 g/cm^3 (8lb/ft^3).

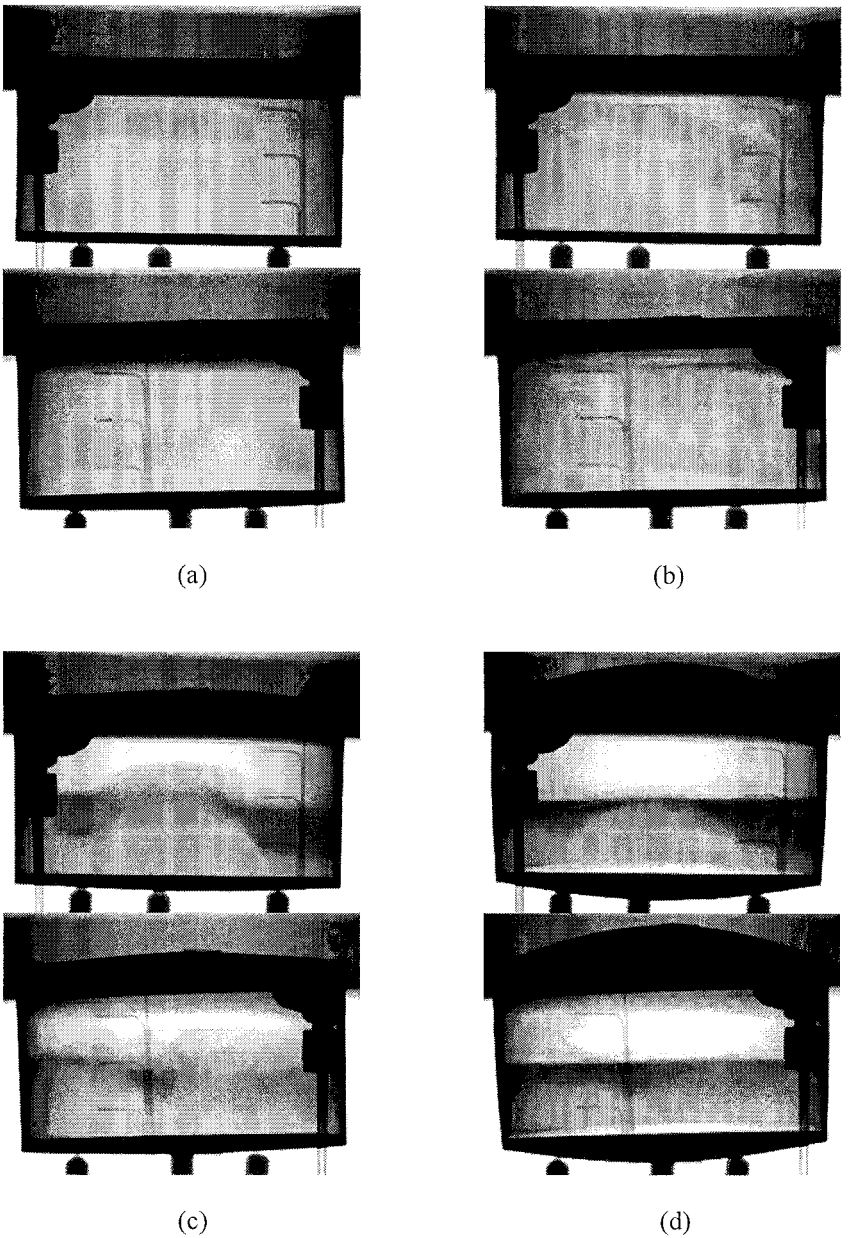

Figure 11: x-ray images from confined REF sample. Bulk density about 0.3 g/cm^3 (20 lb/ft^3)

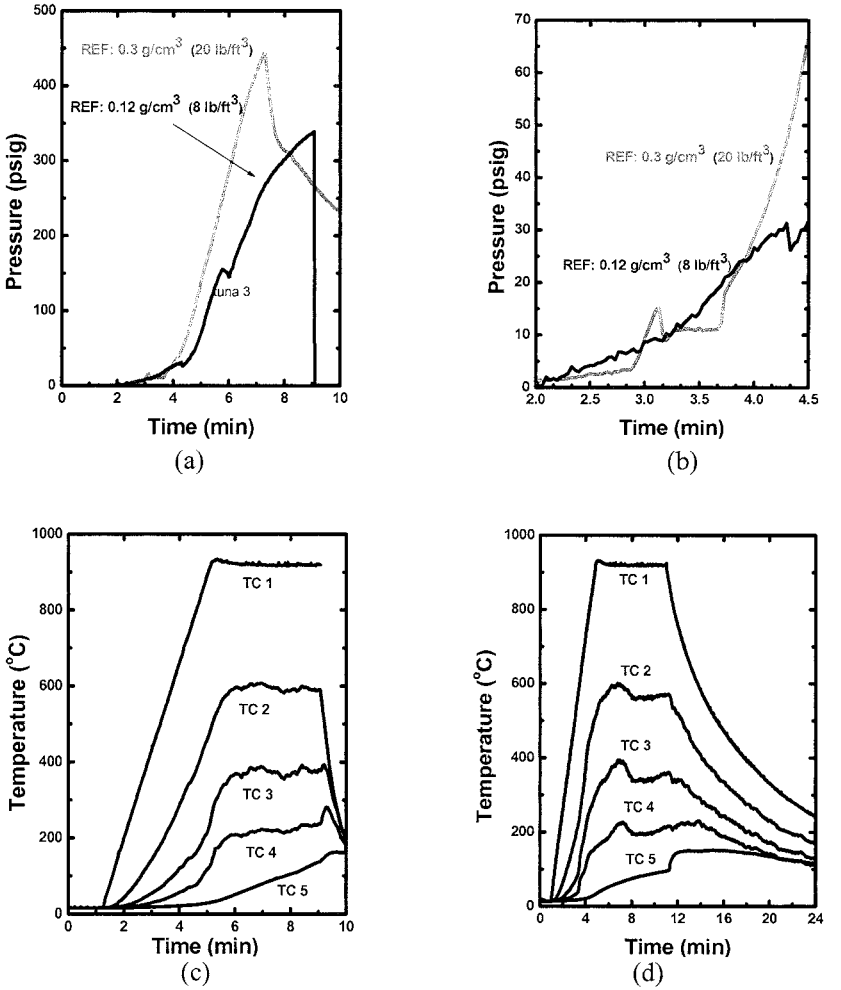

Figure 12: (a) Pressure transducer response, (b) pressure transducer response at early times, (c) thermocouple response for sample in Fig. 10, and (d) thermocouple response for sample in Fig. 11.

Finally, in the case of the sample in Fig. 11, the container yielded gradually at elevated pressure. At some time, which may have occurred after venting, a residue formed in the container. Post-test x-ray imaging shown in Fig. 13 indicated a complicated layered structure that consisted of thin layers of partially decomposed foam (dark gray to black in color) separated by relatively large void regions (having a characteristic dimension on the order of 1 cm). The net result appears to be a complex arrangement of absorbing and re-radiating surfaces, which may have relatively high emissivities (perhaps on the order of 0.8).

Transactions on Engineering Sciences vol 43, © 2003 WIT Press, www.witpress.com, ISSN 1743-3533

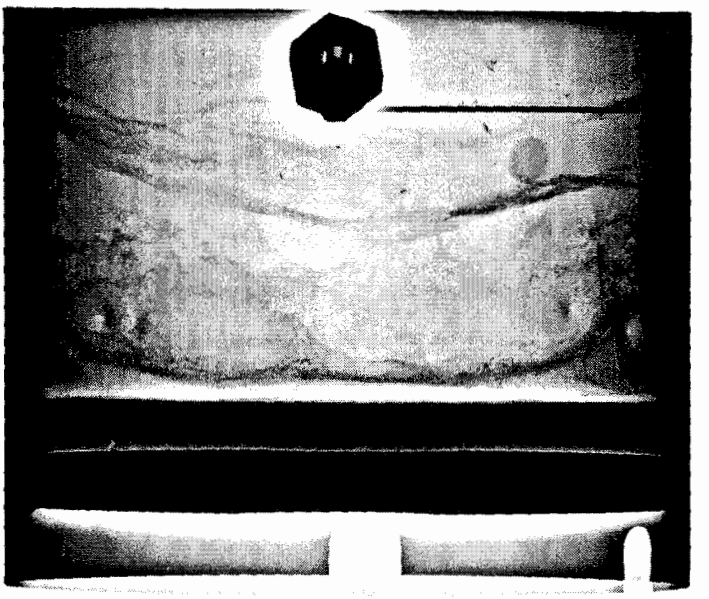

Figure 13: Post-test x-ray image showing layered structure.

3.1.4 Effect of an imbedded mass

Figures 14 and 15 show x-ray images from two experiments from the "XFER" series (Table 1) that involved a relatively large imbedded stainless steel mass (about 370 g) that was surrounded by a foam sample (about 55g). The layer of foam between heated plate and the top of the imbedded mass was 2.54 cm (1 inch) thick. Again, two x-ray cameras were used and were separated by an angle of about 60 degrees. The images from the two cameras have been stacked in Figs. 14 and 15. Both experiments were done with samples in the upright orientation. The power to the heat lamps was controlled so that the temperature of the top plate was ramped (about 180° C/min) to a set point of 900° C and was maintained at that temperature for the duration of the experiment. The container for the sample in Fig. 14 had two vent holes (see Table 1) beneath the heated plate. The foam had a bulk density of about 0.18 g/cm^3 (12 lb/ft^3). The container for the sample in Fig. 15 was sealed so that the container would pressurize as decomposition proceeded. The foam had a bulk density of about 0.12 g/cm^3 (8 lb/ft^3).

Figs. 14a and 15a show the foam samples just prior to the onset of foam regression. Figs. 14b, 14c, and 14d show the regression of the foam at elapsed times of one minute, two minutes and four minutes after the images in Fig. 14a. Figures 15b, 15c, and 15d show the foam regression at similar elapsed times relative to the images in Fig 15a.

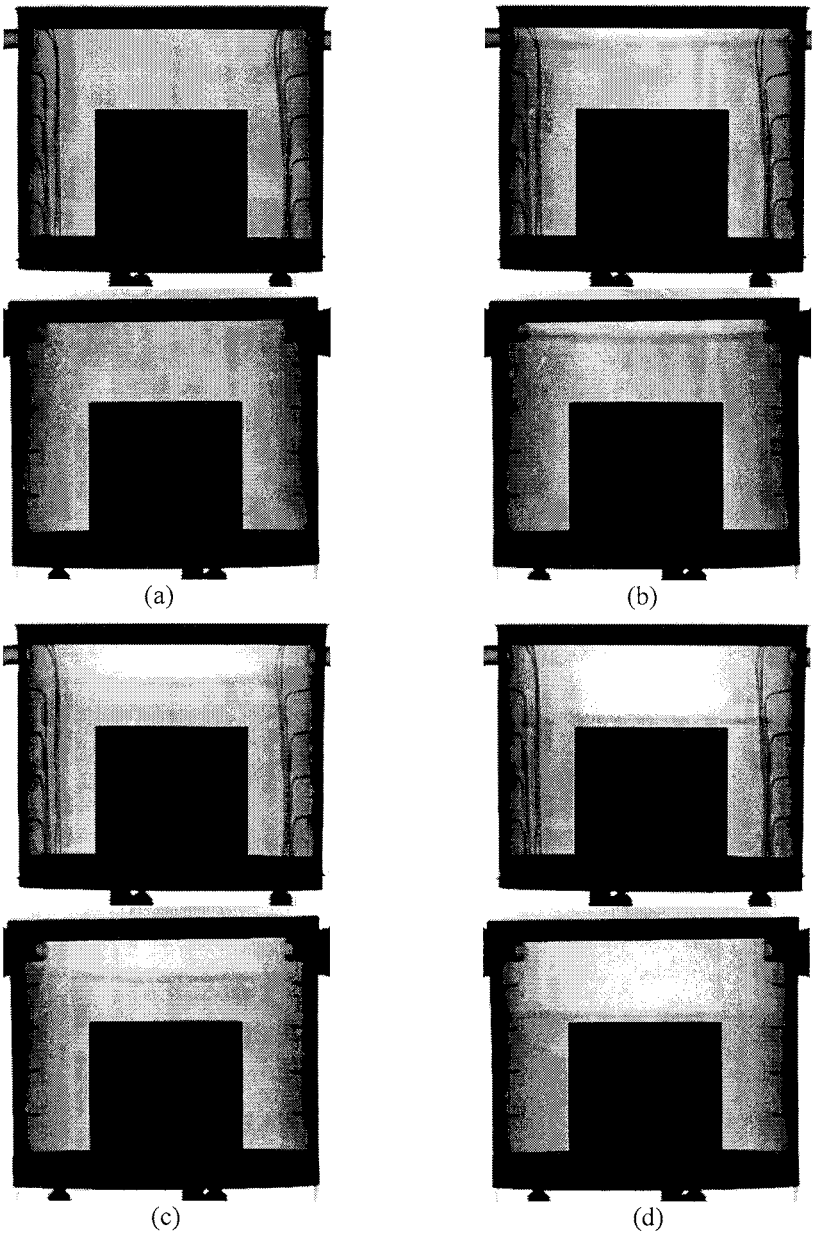

Figure 14: x-ray images from vented sample (foam density about 0.18 g/cm^3) containing an imbedded mass. (a) Immediately prior to regression, (b) one minute elapsed, (c) two minutes elapsed, and (d) four minutes elapsed.

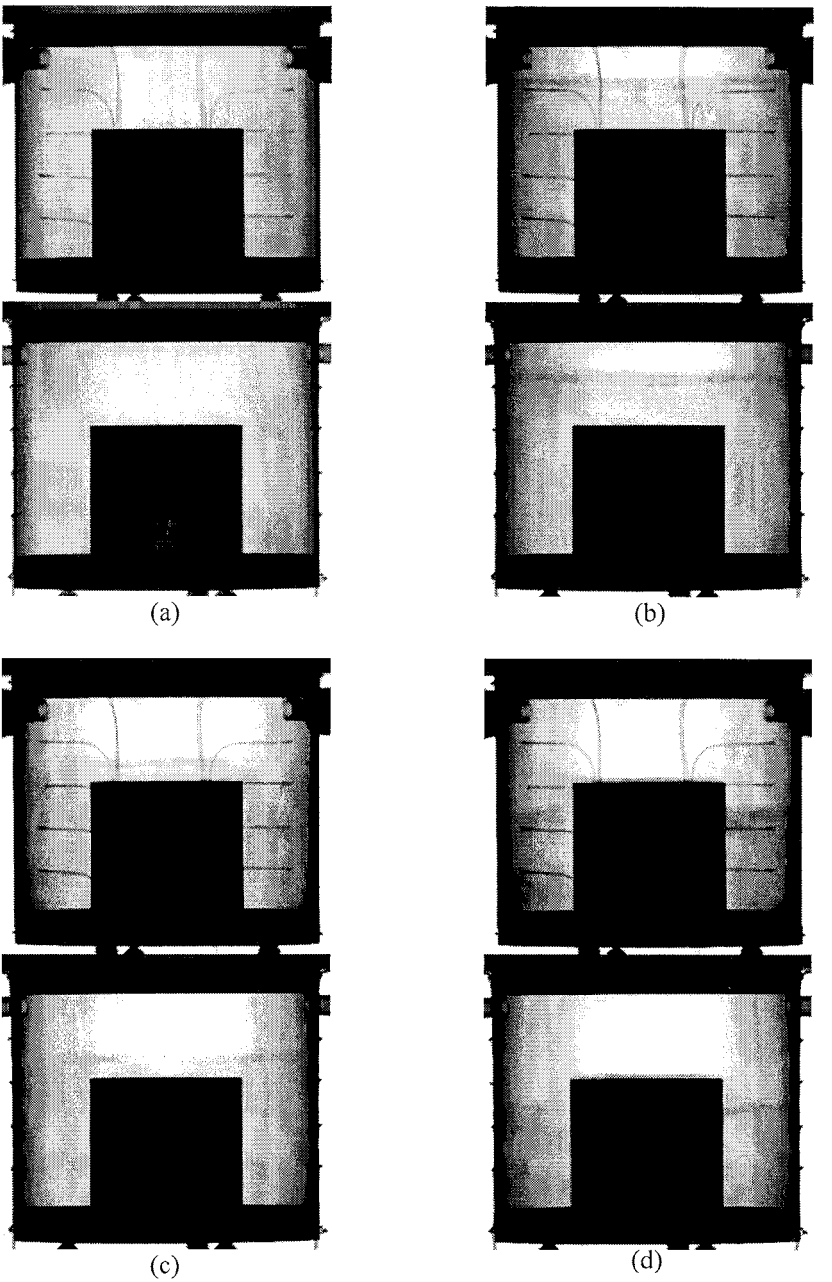

Figure 15: x-ray images from confined sample (foam density about 0.12 g/cm^3) containing an imbedded mass. (a) Immediately prior to regression, (b) one minute elapsed, (c) two minutes elapsed, and (d) four minutes elapsed.

In Fig. 14, the regression front moves relatively rapidly until it reaches the imbedded mass. When the front reaches the top surface of the imbedded mass, regression proceeds much more slowly. The bottom half of the annular portion of the foam was still present after thirty-six minutes. A thin dark region of more dense material formed at the regression front. However, a thick bubbling region did not form as in the well-vented upright configuration shown in Fig 4. This is probably due to the relatively short length of foam between the heated plate and imbedded mass and the higher temperature of the heated plate, which would cause more rapid vaporization of decomposition products. Erosive channeling again occurred with the confined sample in Fig. 15. Unfortunately, the pattern is not discernable in the figure. However, the presence of the imbedded mass slowed overall regression of the foam similarly to the vented sample shown in Fig. 14.

Thermocouples were inserted in the imbedded mass, top and bottom plates as shown in Fig. 16. Thermocouples were also welded to the outside of the containers as shown in Fig. 16.

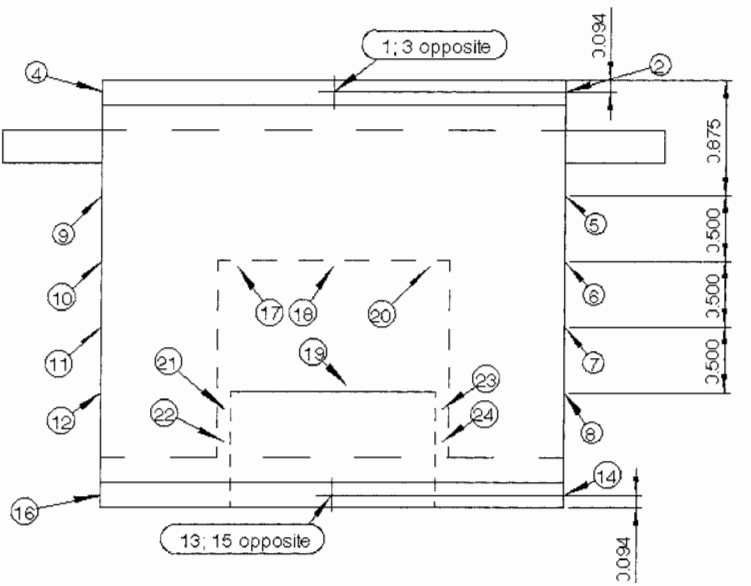

Figure 16: Thermocouple locations for samples shown in Figs. 14 and 15.

The responses of selected thermocouples for the vented sample in Fig. 14 are shown in Fig. 17. Similar thermocouple responses for the confined sample in Fig. 15 are shown in Fig. 18, as well as the response of the pressure transducer. The confined sample pressurized similarly to the confined samples in Figs. 10 and 11. However, the pressure did not increase as rapidly due to the large heat sinking capacity of the imbedded mass.

Layered structures, similar to those shown in Fig. 13, were observed to a greater or lesser extent in most of the experiments with imbedded mass. More work is required to determine the nature of these structures and when they form.

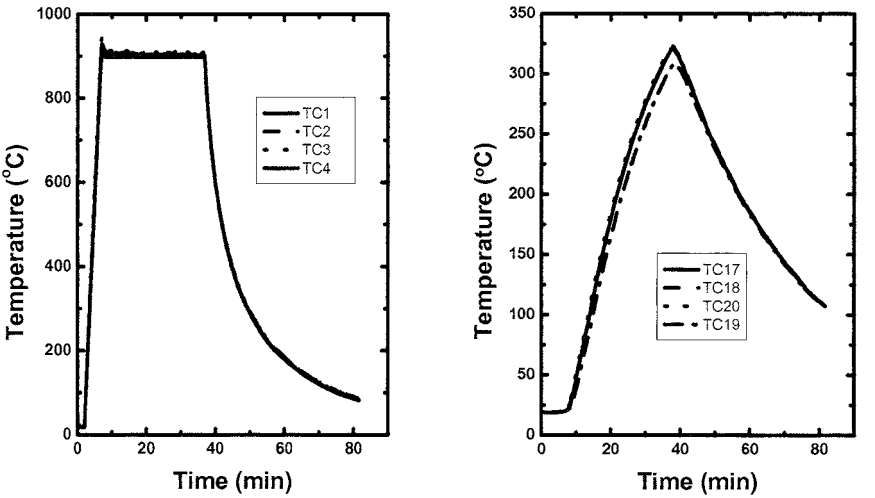

Figure 17: Thermocouple responses for the vented sample in Fig. 14.

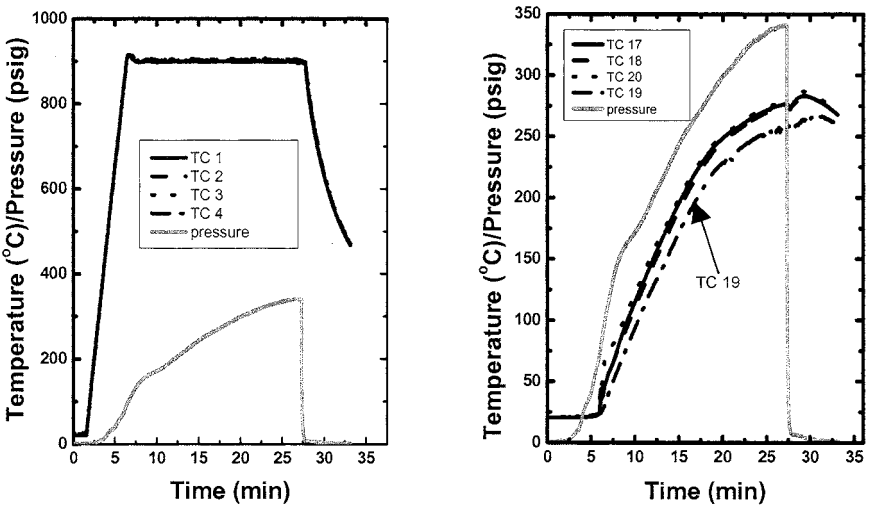

Figure 18: Thermocouple and pressure transducer responses for the confined sample in Fig. 15.

3.2 Laboratory-scale experiments

As mentioned previously, a complete discussion of the laboratory-scale experiments and results are beyond the scope of this paper. However, results from the TGA-FTIR experiments are pertinent to discussion of the results from the production-scale experiments. Therefore, some results from the TGA-FTIR experiments are briefly illustrated below.

Figure 19 shows the percent of sample mass remaining as a function of temperature for both unconfined and partially confined 2.5-mg REF samples heated at 20° C/min to about 575° C. The partially confined sample was contained in a hermetically sealed aluminum pan with a 0.06 mm orifice. Partial confinement has a significant effect on the TGA response. However, FTIR spectra obtained during both experiments indicated little change in the decomposition products that evolved into the gas phase.

Figure 20 shows the rate of mass loss (derivative curves) for the two samples in Fig. 19. The distinct "peaks" in the mass-loss curves indicate multiple reaction steps having different temperature dependencies. From analysis of FTIR spectra and GC-MS analyses several decomposition products have been identified. The most abundant decomposition products in the region of each peak are summarized as follows.

In the temperature range from ambient to about 140° C, the most abundant decomposition products are FC-72, perfluorohexane, with a boiling point (b. p.) of 58° to 60° C, which is the blowing agent in the foam, and some siloxanes, which are believed to associated with the surfactant used in the foam.

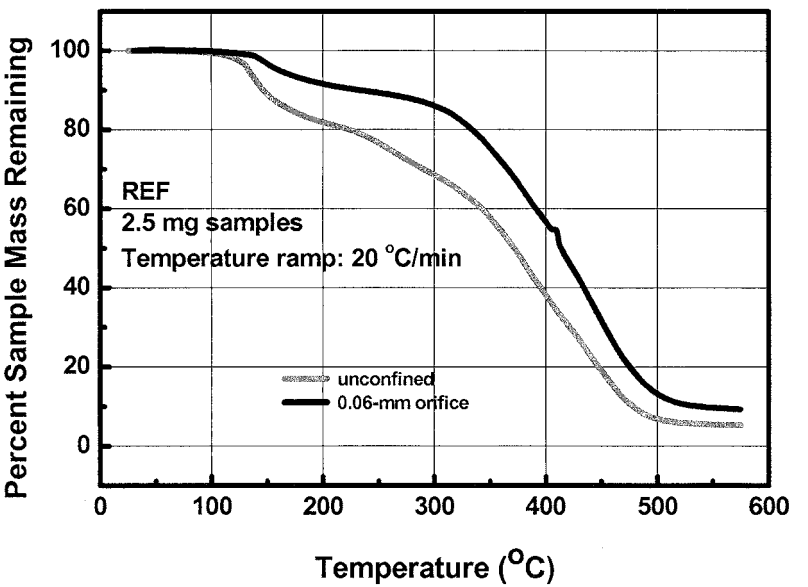

Figure 19: TGA (mass loss) from unconfined and partially confined samples.

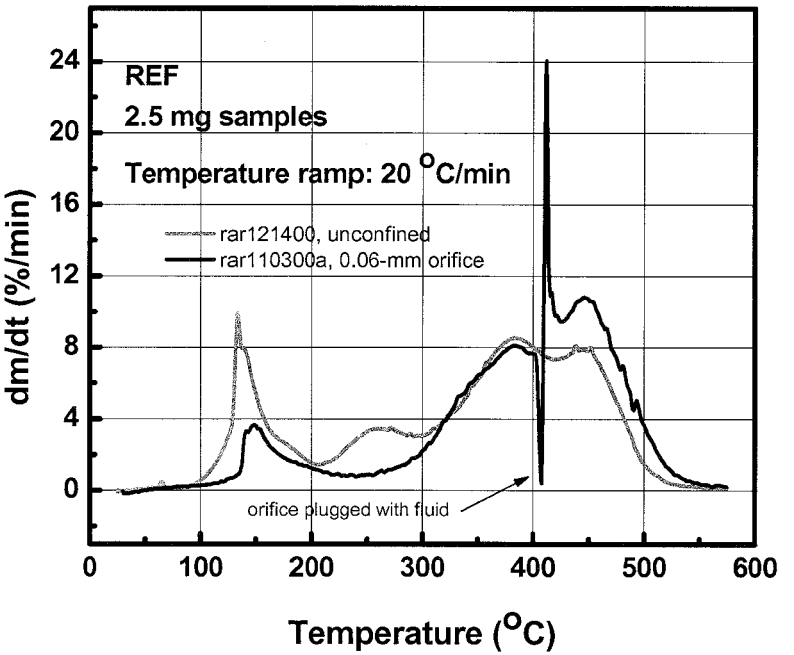

Figure 20: Rate of mass loss from unconfined and partially confined samples.

In the temperature range from about 140 to about 300° C, the major decomposition product is octamethylcyclotetrasiloxane (b. p. 175 to 176° C), which probably is a fragment from the siloxane moiety in the removable resin used to fabricate the foam [1]. Other much less abundant organic products also evolve.

At temperatures above about 300° C, the siloxanes are still observed, but are less abundant. More organic products appear, the identification of which requires further work, although some products have been identified. These include 2-methylfuran (b. p. 63 to 66° C), phenol (b. p. 182° C), toluene (b. p. 111° C), nonylphenol (b. p. 315° C), and bisphenol-A (b. p. 360° C). Nonylphenol and bisphenol-A appear more at temperatures above 350° C, and originate from the commercially available epoxy resin used to fabricate REF [1].

The above discussion of the laboratory-scale experiments is admittedly cursory. However, it should be clear that a variety of decomposition products evolve over different temperature ranges. Most of these products will exert significant vapor pressures at the temperatures observed in the production-scale experiments. This can result in complex mixtures, in which the constituents vary greatly in volatility. Bubble formation and channeling due to pressure gradients are likely to occur as volatile low-molecular weight products evolve in viscous fluid-like phases that can form from high molecular weight polymer fragments and less volatile decomposition products, such as bisphenol-A. The large spike in the derivative curve for the partially confined sample in Fig. 20 was caused by the formation of a fluid phase that temporarily plugged the orifice.

4 Discussion

The results from the production-scale experiments illustrate the bulk behavior that can occur when a polymer-type foam, such as REF, chemically decomposes when subjected to a variety of thermal and physical boundary conditions. Bulk behavior is dominated by both heat and mass transfer. Obviously, the greater the rate of heat transfer is, the more rapidly the foam will decompose. However, the physical behavior of the foam during decomposition, particularly liquefaction and flow, strongly depend on the rate of mass transfer of decomposition products away from or within the system.

The "AF" and "Series 2" experiments (Figs. 4 to 6) illustrate liquefaction and flow under the influence of gravity. As the foam decomposes, lower molecular weight decomposition products evolve and tend to form a fluid phase that exerts a vapor pressure. The amount of liquid present depends on the vapor pressure of the constituents and the rate of mass transfer from the container. As the foam front regresses, heat losses to the ambient (from the walls of the container) increase. The rate of vaporization of decomposition products decreases, and as decomposition continues, liquid accumulates in the container. In the upright case (Fig. 4), the liquid pools on top of the un-reacted foam due to gravity. In the inverted case (Fig. 5), the liquid drains (toward the walls of the container) from the un-reacted foam due to gravity and results in a dome-like structure regressing into the foam. In the side-heated case (Fig. 6), the liquid drains asymmetrically, since the gravity vector is perpendicular to the applied heat flux vector.

The "Tuna" series experiments with a vent opposite the heated plate (Figs. 7 to 9), illustrate the effect of a pressure gradient in system. As liquid forms due to decomposition, that liquid exerts a vapor pressure, which increases with temperature and creates a pressure gradient in the container. The sides of the container are heated by conduction from the heated plate and by radiation within the enclosure. Heating of the side-wall should cause decomposition of the adjacent foam, which would probably create a vapor space favorable to the initiation of a channel. As the fluid that forms exerts its vapor pressure, the vapor will seek the path of least resistance along the side-wall, creating a channel to relieve the pressure.

While it cannot be proven from the x-ray images in Figs. 7 and 8, the most likely mechanism for channeling is probably hot vapor penetrating along the side wall and causing further decomposition, which promotes further vapor penetration, and so forth, until the vapor reaches the end of the container. The TGA-FTIR results discussed above showed that decomposition products will form that can exert substantial vapor pressures. The dark phase that forms during channeling probably results from heat transfer between the vapor and un-reacted foam. Heat transfer would cause decomposition that produces a fluid phase. Furthermore, condensation of the vapor phase would produce additional fluid. As a fluid phase forms, it would create the darker irregular regions seen in Figs. 7 and 8.

Figs. 7 and 8 also show the effect of foam density on the regression rate. Erosive channeling occurs for both densities, however the more dense foam takes much longer to completely decompose due to the additional mass of foam and the energy that must be supplied to cause decomposition.

The "Tuna" series experiments with confined samples (Figs. 10 to 13) further illustrate the prominent effect of erosive channeling. The images shown in Figs. 10 and 11 display substantial asymmetry in the region of foam decomposition. This is probably the result of erosive channeling in a confined system, which would have the maximum amount of a fluid phase present during decomposition. Furthermore, substantial pressurization of the container occurred. This is consistent with the vapor pressures that can be exerted by the identified decomposition products at the temperatures observed in the production-scale experiments. Pressurization was sufficient to cause failure of the stainless-steel containers, and sometimes resulted in an explosion. Figures 10 and 11 further illustrate the effect of foam density on the regression rate, as was discussed above with Figs. 7 and 8.

The "XFER" series experiments with a stainless steel mass imbedded in the foam showed that the presence of an imbedded object could significantly affect foam decomposition. The imbedded mass was a large heat sink that substantially slowed the rate of foam decomposition and regression when the top surface of the mass was exposed to the radiating surface. Again, erosive channeling occurred with the confined sample. Pressurization also occurred, although more slowly. Furthermore, a more subtle interaction may have occurred. The layered structures that formed may have resulted from energy being absorbed by the imbedded object. However, after the layers formed, they probably reduced the radiative heat transfer to both the underlying foam and imbedded object.

5 Summary and conclusions

The behavior of foams, such as REF, that undergo liquefaction can vary greatly depending on both physical and thermal boundary conditions as well as on decomposition chemistry. The production scale experiments illustrated the variety of behavior that can occur with different thermal and physical boundary conditions. Foam regression away from a heated surface generally involves two moving boundaries, a fluid-solid interface and a fluid-vapor interface. In the simplest cases involving well-vented samples and minimum pressure gradients, both interfaces were relatively planar and regressed in a one-dimensional fashion. Similar experiments involving vented samples with pressure gradients or totally confined samples produce complicated three-dimensional interfaces as a result of erosive channeling, probably caused by hot vapors that produced further liquefaction. The presence of an imbedded object with substantial heat sinking capacity can further complicate behavior. In particular, a subtle interaction may occur. Layered structures can form during decomposition, probably at least partially as a result of energy being absorbed by the imbedded object. However, after the layers form, they probably reduce the radiative heat transfer to both the underlying foam and imbedded object. In general, the decomposition processes is very complicated. However, the degree of accuracy required in modeling this processes will depend greatly on the overall accuracy requirements for modeling the engineered system in which the foam is used.

6 Acknowledgements

Sandia is a multiprogram laboratory operated by Sandia Corporation, a Lockheed Martin Company, for the United States Department of Energy under Contract DE-AC04-94AL85000.

The authors gratefully acknowledge the technical assistance provided by the following colleagues at Sandia National Laboratories. The basic experimental technique for the production-scale experiments was developed by T. Y. Chu, John Bentz, and Jack Pantuso. They also performed the "AF" and "Series 2" experiments. The remaining production-scale experiments were performed by Chuck Hanks, Mike Ramirez, Ben Belone, David Ho, and Tomás Sánchez. Jim Nakos provided valuable advise on instrumentation and coordinated activities at the Radiant Heat Facility where the experiments were done. Fabrication of the "Tuna" and "XFER" series experiments was in large part due to the efforts of Paul Thompson and Jo Bridge. Ed Russick and Jim Aubert were responsible for providing the REF samples and also provided technical advise to help understand foam decomposition. Mike Hassard, Jerry Stoker, and Steve Younghouse played key roles in obtaining the x-ray images. John Oelfke instrumented the samples for the "XFER" series of experiments. Jaime Castañeda, Paige Jackson, Anita Renlund, Jill Miller, and Ted Borek made significant contributions to the laboratory-scale experimental program. Tom Fletcher and Dan Clayton of Brigham Young University also played key roles in the laboratory-scale experiments.

Finally, the authors greatly appreciate the technical advice provided by Barry Boughton and Roy Hogan, of Sandia National Laboratories, during the preparation of this manuscript.

References

[1] McElhanon, J. R., Russick, E. M., Wheeler, D. R., Douglas, A. L., Aubert, J. H., Removable foams based upon an epoxy resin incorporating reversible Diels-Alder Adducts. *Journal of Applied Polymer Science*, ***85***, pp. 1496-1502, 2002.

[2] Hobbs, M.L., Erickson, K.L., Chu, T.Y., Modeling decomposition of unconfined rigid polyurethane foam. *Polymer Degradation and Stability*, **69**, pp. 47-66, 2000.